ΔΕΛΤΙΟ ΤΗΣ ΕΛΛΗΝΙΚΗΣ ΓΕΩΛΟΓΙΚΗΣ ΕΤΑΙΡΙΑΣ
Τόμος XLIII, *No* 4

BULLETIN OF THE GEOLOGICAL SOCIETY OF GREECE
Volume XLIII, *No* 4

12ο ΔΙΕΘΝΕΣ ΣΥΝΕΔΡΙΟ
ΤΗΣ ΕΛΛΗΝΙΚΗΣ ΓΕΩΛΟΓΙΚΗΣ ΕΤΑΙΡΙΑΣ

ΠΛΑΝΗΤΗΣ ΓΗ:
Γεωλογικές Διεργασίες και Βιώσιμη Ανάπτυξη

12th INTERNATIONAL CONGRESS
OF THE GEOLOGICAL SOCIETY OF GREECE

PLANET EARTH:
Geological Processes and Sustainable Development

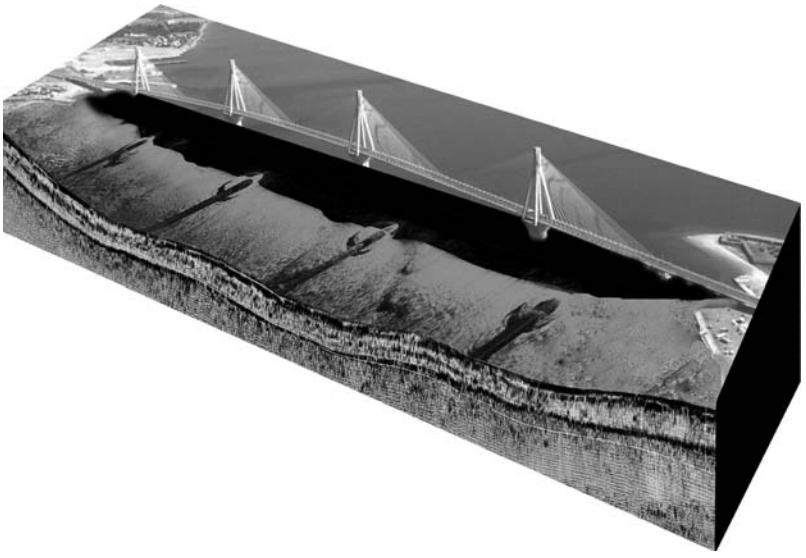

ΠΑΤΡΑ / PATRAS 2010

ISSN 0438-9557

Δελτίο της Ελληνικής Γεωλογικής Εταιρίας, 2010
Πρακτικά 12ου Διεθνούς Συνεδρίου
Πάτρα, Μάιος 2010

Bulletin of the Geological Society of Greece, 2010
Proceedings of the 12th International Congress
Patras, May, 2010

COMPILATION OF A UNIFIED AND HOMOGENEOUS AEROMAGNETIC MAP OF THE GREEK MAINLAND

Chailas, S.[1], Tzanis, A.[1], Kranis, H.[2] and Karmis, P.[3]

[1] *Department of Geophysics – Geothermy, National and Kapodistrian University of Athens, Panepistimiopoli, 15784 Zografou, Greece; schailas@geol.uoa.gr; atzanis@geol.uoa.gr*

[2] *Department of Dynamic, Applied and Tectonic Geology, National and Kapodistrian University of Athens, Panepistimiopoli, 15784 Zografou, Greece; hkranis@geol.uoa.gr*

[3] *Institute of Geology and Mineral Exploration, Geophysics Department, Sp. Loui 1,Olympic Village, 13677 Acharnae – Athens, Greece, karmis@igme.gr*

Abstract

We present a unified and homogeneous digital aeromagnetic map of the Hellenic mainland, based on the 1:50,000 map series of IGME. These maps cover the areas A1, A2, B, C1, C2, C3, D1 compiled by Hunting Geology and Geophysics Ltd. and measured at nominal ground clearances (flight altitudes) 150m AGL, 150m AGL, 300m AGL, and 2300m AMSL respectively (part of C2 with 3000m AMSL). We also include the entire area of Northern Greece, measured by ABEM AB with nominal ground clearance 275±75m AGL. The original map sheets were digitally imaged, georeferenced, digitized along contour lines and interpolated onto regular 250΄250m grids. The unified aeromagnetic map was constructed by collating the mosaic of the resulting gridded data. Using upward/ downward continuation techniques various homogeneous versions of the map, were compiled by referencing of the observed mosaic total magnetic field to a unique constant ground clearance or to a unique constant elevation above mean sea level. This is the first time there is a complete and unified image of the magnetic signature of the isopic zones and rock formations comprising the Hellenic mainland, with particular reference to the ophiolite suites, which provides additional insight into the Alpine and post-alpine tectonics of the area.

Key words: *Greece, aeromagnetic map.*

1. Introduction

The scope of the work reported herein is very clear: To compile a unified and common-referenced aeromagnetic map of Greece, out of the fragmentary information existing in a multitude of 1:50000 scale maps produced by different contractors for the Institute of Geological and Mining Research (IGME).

The original aeromagnetic data set was acquired in two stages: In 1966, ABEM AB conducted a field campaign over Central/ Eastern Macedonia and West Thrace (the hatched area in Fig. 1). In 1977, Hunting Geology and Geophysics Ltd conducted a second campaign extending over West Macedonia, Thessaly, eastern Central Greece, and eastern Peloponnesus (Areas A, B, C and D in Fig. 1). Both contractors delivered the raw data in analogue or digital magnetic tape and the end product in 1:50000 scale contour maps compiled so, as to comply with the corresponding topographic

maps of the Hellenic Army Geographical Survey (HAGS) and the 1:50000 geological maps of IGME.

The "original" 1:50000 scale maps did not comprise a uniform set. Each contractor used different reduction and processing schemes, which resulted in significant inconsistencies at the boundaries between their respective survey areas. Moreover, ground clearance was different between sub-areas surveyed by the same contractor, so that their respective 1:50000 maps were not directly comparable (for details see below). In *several* occasions, when the boundary between two sub-areas surveyed with different ground clearances would straddle a single HAGS/IGME sheet, the *same* 1:50000 aeromagnetic map would be produced with *different* data and contouring schemes (for an example see Fig. 2); this would certainly hinder interpretation and often beget confusion to the novice or unfamiliar with the analysis of potential fields.

National or regional scale maps of commonly reduced and referenced aeromagnetic data for the entire Hellenic territory at different absolute elevations have not been systematically produced. In consequence, regional or spatially extended aeromagnetic anomalies could not be recognized and evaluated. Even local anomalies straddling the boundaries between two maps were discontinued and had to be reconstructed by the interested investigator. Finally, until recently, no information whatsoever existed in some digital form. The only hitherto known attempt to unify a significant subset of the aeromagnetic data and investigate aeromagnetic anomalies at large scales was that of Stampolidis (1999) who *reprocessed* the original flight line data collected by ABEM in Northern Greece.

Inasmuch aeromagnetic surveys aim at the detection of extended – regional scale anomalies and are best suited for strategic scale investigations, the aforementioned limitations and difficulties have hindered their utilization, to the point of leaving a valuable resource mostly unexploited and largely ignored. Herein, we attempt to remedy this situation by producing a unified aeromagnetic map of Greece for the first time and thus bring up an important piece of infrastructure and asset of pure and applied Earth-scientific research.

2. Data Sources

As mentioned above, the compilation of the unified and homogeneous aeromagnetic map of Greece is based on the 1:50,000 map series of IGME, produced by ABEM AB and Hunting Geology and Geophysics Ltd.

The ABEM maps (ABEM, 1967), were produced with measurements at a nominal constant ground clearance (GC) of 275±75m above ground level (AGL) i.e. in constant ground clearance mode. The direction of the flight lines (tracks) was NE-SW and the mean distance between them was about 1km. Connection (tie) lines for crossover adjustment of the data were also flown at NE-SW direction, with a mean distance of 10km.

Hunting Geology and Geophysics Ltd. has generally used a magnetic field measurement spacing of 200–250m and has flown on a NE-SW direction, but at different GC's and track densities depending on the topography. The data collection schemes are as follows (also see Fig. 1):

- Area A1 (Thessaloniki basin): Nominal GC 150m AGL at a nominal distance of 400m between tracks.
- Area B (Thermaikos Gulf): Nominal GC l 150m above mean sea level (AMSL) at a nominal distance of 400m.
- Area C1 (Paikon Mountain): Nominal GC 300m AGL at a nominal distance of 800m.

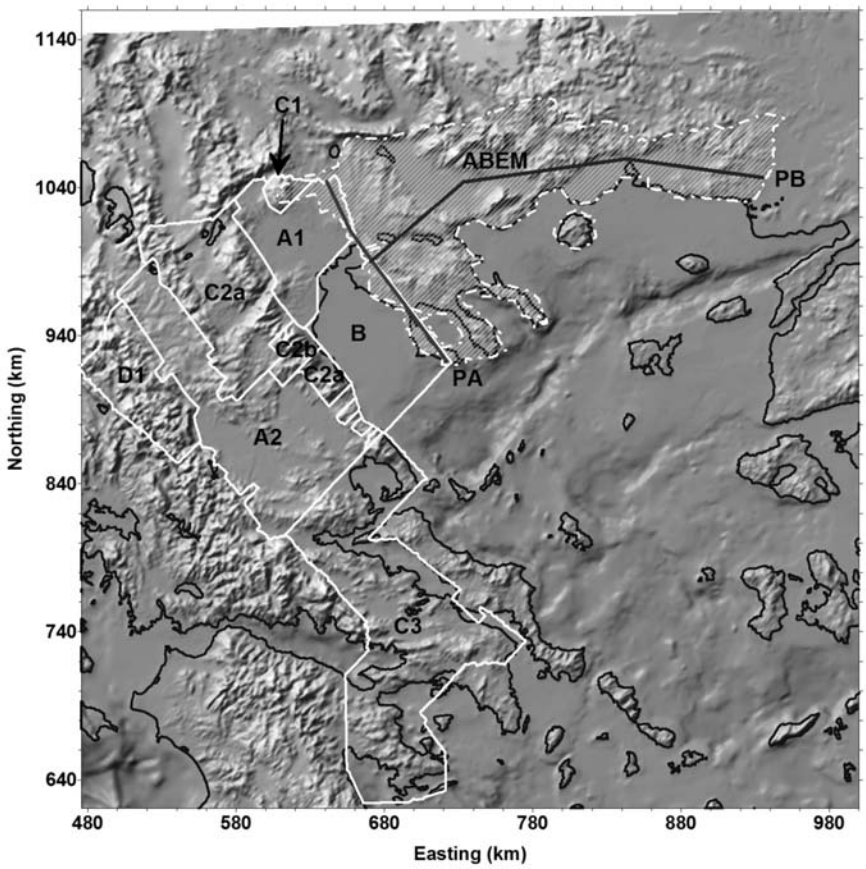

Fig. 1: Map showing the area coverage of the aeromagnetic data.

- Area C2a (the highlands between Thessaloniki and Thermaikos basins to the east and the Pindus Mt. chain to the west, including the Florina and Ptolemais basins): Nominal GC 300m AGL at a nominal distance 800m between tracks.
  - Exception is the area of Mt. Olympus, (area C2b) where the flight level was 3000m AMSL with the same nominal distance between lines.
- Area A2 (the Mesohellenic trough and the Karditsa and Larissa basins): Nominal GC was 150m AGL at a nominal distance of 400m.
- Area C3 (Eastern Central Greece): Nominal GC 300m AGL at a nominal distance of 800m.
- Area D1 (the Pindus Mt. chain): Nominal flight level was 2300m AMSL at a distance of 1000m between tracks.

In all cases, connection lines were flown at a NE-SW direction and a spacing of 10km. The IGRF correction was based on the IGRF model for the epoch 1977.3. A constant value of 150nT was added to the magnetic anomaly values prior to plotting the contour maps. It is probably worth noting that the original raw data set delivered by Hunting Ltd in magnetic tapes, has been irreversibly damaged and all that was left from this important survey are the 1:50000 contour maps.

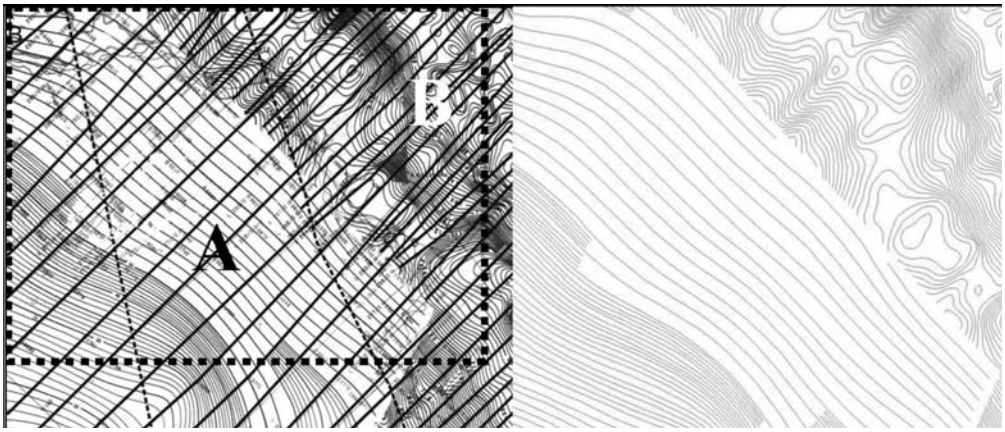

Fig. 2: Left: Part of the aeromagnetic map of sheet 'Kalampaka', scale 1:50.000.The continuous NE-SW lines indicate the primary flight lines and the dashed NW-SE lines the connecting (tie) lines. Area A was measured at a constant ground clearance of 2300m and flight line spacing of approx. 1000m Area B was measured at a cgc of 150m, with flight line spacing 400m. The change in the detail and the appearance of local anomalies is evident. Right: The digitized contour lines for the inset rectangle faithfully reproduce the original map.

3. Digitization and Gridding Procedure

The original 1:50000 map sheets were initially converted to a high resolution raster image format (typically TIFF). The contour lines were then digitized to vector form (image coordinates) with sufficiently high sampling densities, so as to faithfully reproduce the original image. Fig. 2 shows a part of an original map in raster format (left) and the resulting plot of the digitized contours. The boundaries between neighbouring areas with different flight parameters were also digitized. Using the corners of the map sheets as control points, the map were georeferenced and the image coordinates were transformed to Cartesian coordinates in the UTM projection. The digitized contour lines were subsequently stored in area-files according to the data collection schemes (flight line characteristics) detailed of Section 2. The area files were then interpolated to a regular grid, using a grid spacing of 250m.

The selection of the grid spacing was an exercise in optimal compromise and deserves some attention. First, let it be noted that the magnetic measurements along flight lines were taken at intervals of the order of 200m and certainly £250m. In consequence:

1. This interval is directly comparable to the flight line spacing of 300m for areas measured at 150m AGL. When projected to a direction perpendicular to a flight track, the distance is approx. 353m, longer than the nominal distance between lines. This ensures the faithful reproduction of the local aeromagnetic anomalies.
2. For lines flown 800 and 1000m apart (areas measured at 300m and 275m AGL respectively), the projection at a direction perpendicular to the line is respectively 44% and 35% the distance between flight tracks. This is just sufficient to ensure reproduction of aeromagnetic anomalies with minimal noise (interpolation artifacts) at short wavenumbers.
3. For track lines spaced 1000m and 800m apart and flight levels 2300m and 3000m respectively, the measured field is already smooth enough, to ensure that short wavenumber artifacts will not be introduced during interpolation.

On collating the mosaic of the resulting gridded areas to build a first draft of the aeromagnetic map,

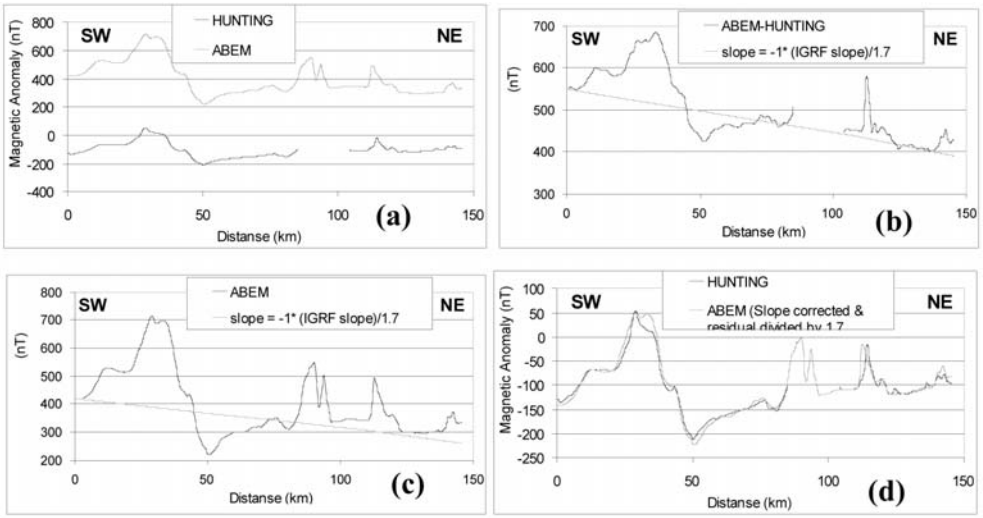

Fig. 3: (a) The total magnetic field along the profile PA in the overlapping region of the ABEM and Hunting survey areas (see Fig. 1). (b) Plot of the difference between the profiles of Fig. 3a. The trend line was calculated as a scaled function of the IGRF slope along the profile. (c) Plot of the ABEM profile with similarly calculated trend line. (d) The profiles of Fig. 3a after reduction of the ABEM data for the trend and scaling for the 1:1.7 distortion factor (see text for details).

we observed an offset of ~450nT (mean datum value) between the Hunting and ABEM data sets in the region where areas A and C1 C2 overlap (Fig. 1 and Fig. 3b), which could not be attributed to the ~125m difference in the flight level: although ABEM was flying higher than Hunting, their contoured magnetic field values were already higher than those of Hunting! In order to investigate the reasons behind the difference of the two data sets, a SW-NE profile was sliced from both data sets across the overlapping region (profile PA in Fig. 1). As can be seen in Fig. 3a, the same local magnetic features are present in both profiles, but the ABEM data is not only upwards offset, but also appears to be vertically exaggerated! Subtraction of Hunting's values from ABEM's profile revealed the existence of a regional trend in the differences (Fig. 3b). Comparing these differences with the slope of the IGRF model for the epoch 1966.5, we found that the trend line is actually a scaled version of the IGRF with a ratio equal to 1:1.7. We have also found that this trend can be *exclusively* attributed to the ABEM data (Fig. 3c). After subtracting the trend from the ABEM profile and scaling the residual curve, the Hunting and ABEM profiles have practically coincided (Fig 3d). The discrepancy between the Hunting and ABEM maps can therefore be attributed to a distorted (erroneous) IGRF correction of the ABEM data.

The first draft of the "unified" Greek aeromagnetic map was constructed by collating the mosaic of the gridded areas, after correcting the ABEM data for the offset of 450nT and the Hunting data for the constant of 150nT added prior to plotting. The result is shown in Fig. 4. It is immediately apparent that the boundaries between different areas are discontinuous and the texture of the map inhomogeneous and different between different survey areas, as a result of the differences in the data acquisition procedures.

An additional observation is that the ABEM data exhibit a persistent eastward downward slope. The comparison of the map of Fig. 4 with the aeromagnetic map of Turkey (Akin, 2007; comparison is not presented herein) has also shown differences of the order of 200nT at the boundaries. Given the analysis presented above for the differences between the Hunting and ABEM data, it would appear

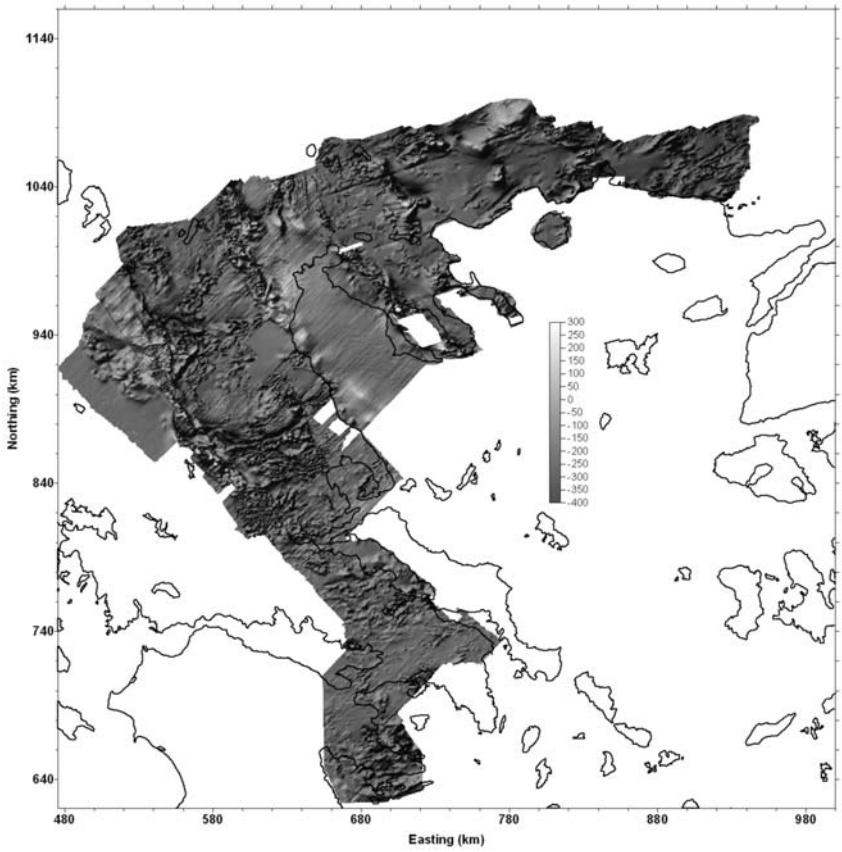

Fig. 4: The mosaic aeromagnetic map produced by digitizing the 1:50.000 scale aeromagnetic maps by Hunting Ltd and ABEM AB. A constant value of 450nT has been subtracted from the ABEM data and a constant value of 150nT from the Hunting data; the latter has been arbitrarily added prior to plotting. The obvious discontinuities across area boundaries are due to the different data collection schemes (see Section 2). The eastward downward slope observed in the ABEM data is due to a distorted IGRF correction (see text for details).

that the same distorted IGRF correction is to blame for the downward slope, as well as for the discrepancy between the Greek and Turkish data. In order to confirm the effect, we have constructed a W-E profile along the ABEM area, as shown in Fig. 1 (profile PB). The profile is plotted in Fig. 5a, together with the trend line calculated as a scaled version of the IGRF model for the epoch 1966.5, in the same manner as per Fig. 3c. Fig. 4d shows the same profile before (continuous black line) and after de-trending and re-scaling (continuous grey line). It is apparent that the original and corrected profiles exhibit a difference of approx. 200 nT at the east end of the profile, approximately the same as the difference observed between the Greek and Turkish data. It is therefore confirmed that the aeromagnetic contour maps delivered by ABEM are distorted. The actual reason for this distortion is still not known, but the previous analysis indicates, either incorrect reduction of the data, or a recorder calibration error. What is important however is that the effect has been recognized and may be reversed using the procedure described above.

The map of Fig. 4 is certainly unified, inasmuch as this is the first time that the mosaic of the different aeromagnetic surveys over mainland Greece has been put and presented together. At the same

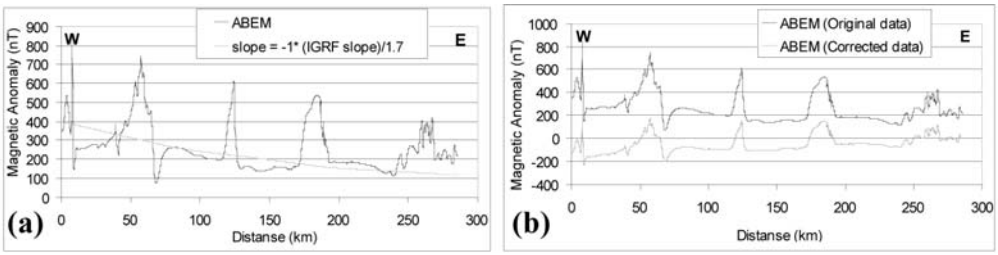

Fig. 5: (a) An E-W profile sliced from the ABEM data (Profile PB in Fig. 1). The trend line has been determined as per Fig. 3c. (b) The same profile before and after de-trending and re-scaling as per Fig. 3d.

time, it is very inhomogeneous and unusable for strategic planning and extended/ regional scale studies! In this form, it is only useful for the analysis of local or extended aeromagnetic anomalies limited to within areas of uniform data collection schemes (see Fig.1 and Section 2). Moreover, the ABEM data require additional processing (de-trending and re-scaling) in order to represent the true amplitudes of local aeromagnetic anomalies. The homogenization of the mosaic map of Fig. 4 leading to the construction of the first complete aeromagnetic map of mainland Greece is presented in the following Section 4.

4. Homogenization

As mentioned previously, by "homogenization" of the mosaic map of Fig. 4, we imply the reference of the entire map to a common and *unique* constant ground clearance, or to a *unique* elevation AMSL. This is an exercise in upward/ downward continuation with the added difficulty that the observation surface (flight altitude) is not flat – the aircraft flew at a constant clearance (height) above the ground surface, following the contours of the terrain. Thus, direct methods of up- or downward continuation assuming flat observation surfaces (e.g. Fourier-based) cannot be applied because the magnetic field intensity obeys an inverse square attenuation law. We need to apply continuation of the field between arbitrary surfaces and in such cases the method of choice is the method of equivalent sources.

We have chosen to use the highly accurate and computationally efficient approach described by Xia et al (1993). This is a two-stage procedure: The first step requires the computation of an equivalent source layer at a horizontal surface below the lowest elevation of the observation and continuation surfaces. The layer is in fact a grid of sources which is iteratively assigned with a distribution of magnetizations through forward calculation of the anomaly on the observation surface, so as to faithfully reproduce the observed total magnetic field. In a second step, the field is up- or downward continued to any arbitrary surface by forward computation on the basis of the equivalent source layer.

In our case, the exact observation surface (flight contour) is not known, but may be approximated to arbitrary precision on the basis of a digital elevation model (DEM). Herein, we have used a 100´100 m DEM based on the 1:50.000 scale maps of the HAGS. The DEM grid was re-interpolated to the nodes of the aeromagnetic grid and the appropriate adjustments were applied at each node, in order to reproduce the ground clearance parameters of the area at which the grid point belongs.

On the basis of the thusly approximated observation surface, the procedure of Xia et al (1993) was applied separately for each area described in Section 2 and the final "unified and homogeneous" aeromagnetic map was constructed by collating the mosaic of up- or downward continued grids, commonly referenced to a *unique* constant ground clearance, or to a *unique* elevation AMSL. Prior to upward continuation, the ABEM data was de-trended and re-scaled according to the procedure of

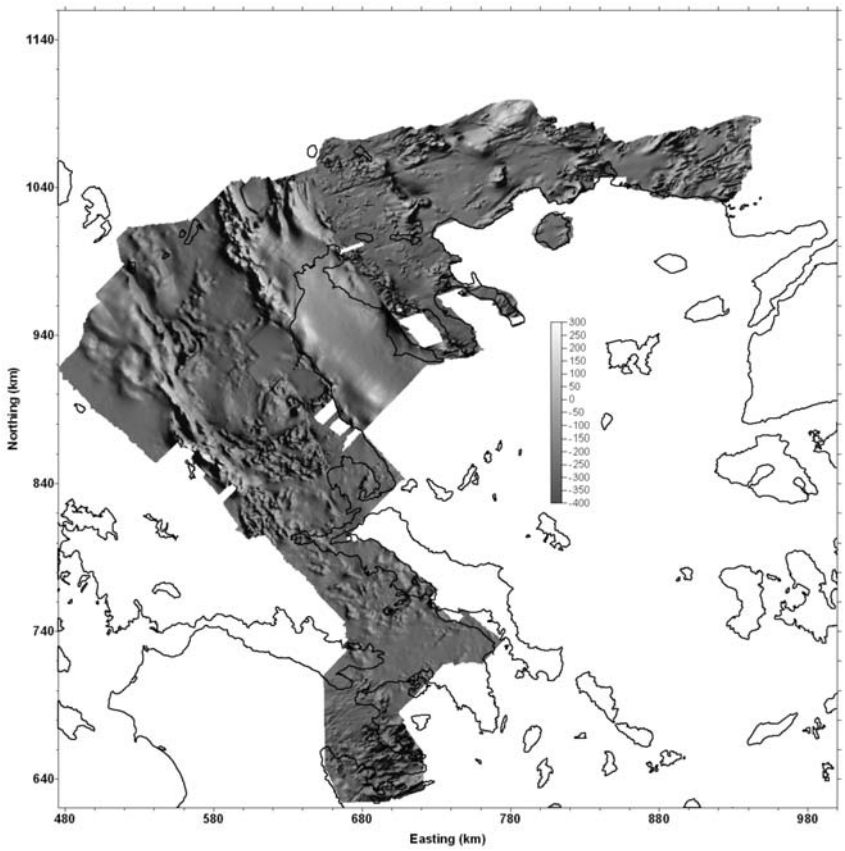

Fig. 6: The aeromagnetic map of the Hellenic mainland homogenized at 300 m AGL In this final product the ABEM data have been de-trended and re-scaled according to the discussion of Section 3. The map is presented in shaded relief form, lit from the NW.

Section 3, in order to correct for the distorted IGRF correction and the resulting grid was adopted only after demonstrating compliance with the Hunting and Turkish data.

Herein we present two versions of the unified and homogeneous map. Fig. 6 illustrates the map at a *constant ground clearance* of 300m AGL and Fig. 7 is the same, upward continued to a *constant altitude* of 3000m AMSL. Both maps are presented in the form of a shaded relief lit from the NW, in order to accentuate their respective characteristics and facilitate the brief discussion to be presented in Section 5.

5. Brief Discussion and Conclusions

The unified and homogeneous maps presented herein show for the first time, a complete and unified image of the crustal magnetic field at regional – national scale. In these images, the signatures of many isopic zones and rock formations comprising the Hellenic mainland are clearly seen, with particular reference to the ophiolite suites. Thus, a different and very interesting glimpse at the Alpine and post-alpine tectonics of the Hellenic territories is possible.

To begin with, the aeromagnetic data roughly delineate the boundaries of isopic zones, or groups of isopic zones. Thus, from east to west, the following groups of zones can (more or less) clearly be

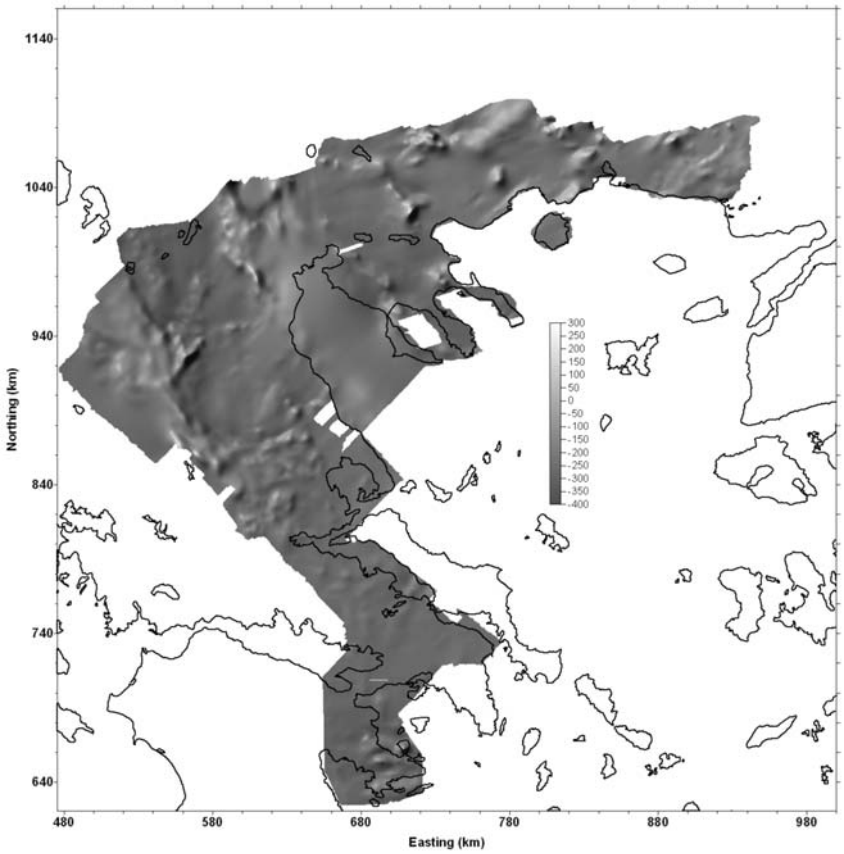

Fig. 7: The aeromagnetic map of the Hellenic mainland homogenized at 3000 m AMSL In this final product the ABEM data have been de-trended and re-scaled according to the discussion of Section 3. The map is presented in shaded relief form, lit from the NW.

defined: (a) The Rhodope massif; this can be distinguished from the Circum-Rhodope belt at the SE of Evros due to the remarkable roughness of the magnetic terrain observed there, presumably due to tectonism. (b) The Serbomacedonian massif; (c) the Circum-Rhodope and Peania zones; (d) the Paikon and Vardar zones; (e) the Pelagonian and Sub-Pelagonian zones.

These groups of zones are mainly differentiated (bounded) by the emplacement of intrusive rocks, especially at northern Greece and, mainly, the emplacement of ophiolite suites. Conversely, the Pindos and Gavrovo zones at the W-NW end of the map and glimpses of the Parnassus zone stand out because of the low to very low magnetizations of their associated stratigraphic sequences.

The magnetic signatures of the ophiolite sequences of the Pelagonian and Sub-pelagonian zones deserve some attention and will be briefly commented starting at the north. The magnetic signature of the Pindos ophiolites appears stronger than those of Vourinos, which according to Papanikolaou (2009) belong to the H4 Axios-Vardar terrane. This may suggest that the Vourinos and Pindos ophiolites do not link beneath the sediments of the Mesohellenic Trough, as proposed by Rassios et al. (1983) and Jones & Robertson (2001). A conspicuous, NE-SW anomaly is observed north of Kalambaka, marking, more or less, the northern boundary of Mt Antihasia. Quite interestingly, it lays on the SW-prolongation of the Aliakmon – Servia Fault Zone and also marks the southernmost bound-

ary of the Vourinos ophiolites.

An arcuate "trough" can be seen, passing east of Karditsa, marking the northern limit of Mt Phyllion and reaching close to the SW flanks of Mt Ossa. It separates the southern part of the Thesally basin from the northern one. Within the former, the Tertiary and Quaternary sedimentary cover appears to be considerably thinner, while the underlying alpine occurrences appear intensely dismembered and dissected by NW-SE, NE-SW and probably E-W tectonic contacts (faults). Actually this area appears to be also bounded on the east by a NNW-SSE discontinuity, the nature of which is at present enigmatic. A little further to the south, a practically straight, ENE-WSW discontinuity marks the southern margin of the Thessaly plain. It can be traced from the Nea Anchialos on the NW part of Pagasitikos Gulf to Domokos and it coincides with the Nea Anchialos Fault, which marks the northern boundary of the Almyros Basin (Caputo & Pavlides, 1993), locus of several earthquakes in the previous century (Papadimitriou & Karakostas, 2003). It is also noteworthy that this ENE-WSW discontinuity seems to change polarity, as at its eastern part (Almyros basin) it appears to be a steep, south-dipping fault, while in the west, the downthrown block is the northern one, corresponding to the Karditsa plain.

The area of eastern Central Greece (Sterea Hellas) is weaved with an intricate pattern of intermediate amplitude anomalies due to an ophiolite sequence dismembered and dissected mainly by NW-SE, NE-SW faulting. The nature of these features has recently been discussed by Tzanis et al (2010). Finally, the magnetic signatures of (Sub-pelagonian) rocks at the Argolis peninsula in central-eastern Peloponnesus is also quite rough, with prevailing E-W and NW-SE discontinuities, the nature of which is yet to be determined.

Returning to northern Greece, the signature of the Axios-Vardar ophiolites, as well as the boundaries of this ophiolite suture are clearly discernible, both inland and offshore, in the Thermaikos Gulf. The strong, indented anomaly on the western margin of the Strymon half-graben does not seem to correspond to the inferred fault that bounds the basin on the west, which develops on the hanging-wall of the Strymon Valley Detachment (Dinter, 1998). Instead it appears to be related to the boundary between the Vertiskos and Kerdyllia Units, (Papanikolaou, 1993). Another interesting observation is that the high-angle, NW-SE normal faults that bound the Strymon and Drama basins are not directly identifiable in the aeromagnetic map. Some tertiary intrusive bodies appear to have stronger magnetic signature than others. For example, the Vrondou pluton, north of Serrai, stands out very clearly, while the Symvolon granite, west of Kavala is less prominent. However, even in this latter case, its boundaries, which are related to the major Kavala-Xanthi-Komotini Fault (KXK), are seen as extended linear "troughs" oriented NE-SW and most probably correspond to the Symvolon Shear Zone, according to Dinter (1998). A structure of similar orientation (NE-SW) is also observed at the delta of Nestos River, parallel to the present-day coastline. This zone may also correspond to a sheared block, related to the KXK or a structure parallel to it. As a matter of fact, further to the east, in the Alexandroupolis- Evros area, several NE-SW to ENE-WSW lineations, most probably related to faults with predominant strike-slip character, can be observed. A high-intensity 'islet' is located at the south-eastern part of the Drama supradetachment half-graben. This feature may be related to a buried intrusive body, related to the Symvolon granite, which has been cut off and displaced by the combined activity of the KXK and the Drama Faults (see Stampolidis and Tsokas, 2004 for additional information). Between Xanthi and Porto Lago, the observed high magnetic values may equally be related to buried intrusive bodies; this, in turn, can be associated with the Nea Kessani geothermal field (Kolios et al., 2005). It is also worth noting that while many linear features can be directly associated with faulting as discussed above, others may not be as easily explainable. A prime example is the long NE-SW lineament parallel to the Greek-Bulgaria border along the line Mavrovouni – Falakron – West Rhodope Mts., whose nature is at present a mystery!

To conclude our brief presentation, we note that herein we have presented the first regional – national scale digital maps of homogeneous aeromagnetic data at different reference surfaces. As shown in the brief discussion above, these maps offer the opportunity to conduct studies of regional or spatially extended aeromagnetic anomalies, as well as local, kilometric scale anomalies; this was hitherto not feasible with the existing inhomogeneous, printed 1:50000 scale map series. Inasmuch as the aeromagnetic maps are principally used for the analysis of extended – regional scale features and strategic planning, the new set of maps contribute an important piece of geo-scientific infrastructure and the opportunity to utilize a valuable resource for pure and applied geophysical and geological research.

6. Acknowledgements

The authors would like to thank Professor G. Tsokas for kindly reviewing the manuscript.

7. References

ABEM, 1967, Final Report on an Airborne Geophysical Survey carried out for the Greek Institute for Geology and Subsurface Research during the year 1966 by ABEM-AB Elektrisk Malmletning, Stockholm

Akin, U., 2007. Aeromagnetic Map (Total Intensity) of Turkey, General Directorate of Mineral Research and Exploration, Ankara, Turkey

Caputo, R. & Pavlides, S., 1993. Late Cainozoic geodynamic evolution of Thessaly and surroundings (central-northern Greece). *Tectonophysics*, 223, 339-362.

Dinter, D., 1998. Late Cainozoic extension of the Alpine collisional orogen, north-eastern Greece: Origin of the north Aegean basin. *Bull. Geol. Soc. America*, 110, 1208-1230.

Jones, G., Robertson, A.H.F., 1991. Tectono-stratigraphy and evolution of the Mesozoic Pindos Ophiolite and related units, Northwestern Greece., *J. Geol. Soc. London* 148, 267– 288.

Kolios, N., Koutsinos, S., Arvanitis, A., Karydakis, G., 2005. Geothermal Situation in North-eastern Greece, Proc. World Geothermal Congress Antalya, Turkey, 24-29 April 2005, 1-14.

Papadimitriou, E. & Karakostas, V, 2003. Episodic occurrence of strong (M_wv6.2) earthquakes in Thessalia area (central Greece). *Earth Plan. Sci. Let.*, 215, 395-409.

Papanikolaou, D., 1993. Geotectonic evolution of the Aegean. Proc. 6th Congress of the Geological Society of Greece, *Bull. Geol. Soc. Greece*, 28/1, 33–48.

Papanikolaou, D., 2009. Timing of tectonic emplacement of the ophiolites and terrane paleogeography in the Hellenides. *Lithos*, 108, 262-280.

Rassios, A., Beccaluva, L., Bortolotti, V., Moores, E.M., 1983. The Vourinos ophiolite complex. *Ofioliti* 8, 275– 292.

Stampolidis, A., 1999. The Geomagnetic field in Macedonia and Thrace and its relationship with the geophysical and geological structure of the area, Doctoral Dissertation, Aristotelian University of Thessaloniki, 258pp (in Greek).

Stampolidis, A. and Tsokas G., 2004. Location of magnetic contacts and depth estimates for the magnetic sources from the aeromagnetic data of Macedonia and Thrace, Proceedings of the 10th Int. Congress, Thessaloniki, April 2004, in *Bull. Geol. Soc. Greece*, vol. XXXVI, 1252 – 1261 (in Greek).

Tzanis, A., Kranis, H. and Chailas, S., 2010. An investigation of the active tectonics in central-eastern mainland Greece, with imaging and decomposition of topographic and aeromagnetic data. *J. Geodyn.*, 49, 55 – 67 (doi:10.1016/j.jog.2009.09.042).

Xia, J., Sprowl, D.R. and Adkins-Heljeson, D., 1993. Correction of topographic distortions in potential-field data: A fast and accurate approach; *Geophysics*, 58(4), 515-523

Δελτίο της Ελληνικής Γεωλογικής Εταιρίας, 2010
Πρακτικά 12ου Διεθνούς Συνεδρίου
Πάτρα, Μάιος 2010

Bulletin of the Geological Society of Greece, 2010
Proceedings of the 12th International Congress
Patras, May, 2010

A MATLAB PROGRAM FOR THE ANALYSIS AND INTERPRETATION OF TRANSIENT ELECTROMAGNETIC SOUNDING DATA

Andreas Tzanis

University of Athens, Department of Geophysics and Geothermy, Zografou 15784, Greece, atzanis@geol.uoa.gr

Abstract

Herein we present a software system, written in MATLAB, to interpret TEM sounding data. The program, dubbed maTEM, is designed to process, model and invert multiple soundings, either individually, or simultaneously along profiles. The latter capability allows for laterally constrained inversion, so as to generate pseudo-2D or 2D resistivity sections based on the program EM1DINV v2.13 by the Hydro-Geophysics Group of the University of Aarhus, Denmark. Using maTEM, the analyst may import and display data multiple data sets, denoise and smooth the data, perform approximate inversions, design 1-D model(s) graphically, perform forward modelling and inversion and generate/ update data base in which to store the results. Finally, the analyst may use the data base to create 2-D and 3-D displays of the geoelectric structure with built-in graphical functions. maTEM is highly modular so that additional functions can be added at any time, at minimal programming cost. Although the software presented herein is focused on the analysis of TEM data, the maTEM concept has been designed ready to incorporate additional electrical and EM geophysical sounding methods and to mutually constrained analysis of different geophysical data sets.

Key words: *Electromagnetic sounding, TEM, MATLAB, geophysical interpretation.*

1. Introduction

The Transient Electromagnetic (TEM) exploration method is becoming increasingly popular for its effectiveness and robustness in hydrogeological, environmental, engineering geological applications, as well as general geological and geophysical mapping. In fact, due to its sensitivity in resolving small contrasts in generally highly conducting structures, it has become the EM method of choice for such applications, as the detection and mapping of subterranean water concentrations and flow paths, detection and monitoring of salination processes in coastal aquifer systems, detection and monitoring of aquifer pollution and pollutant migration, detection and mapping of buried faults, deep lifelines, leakage, UXO etc.

A pre-requisite for TEM applications in hydrogeological and environmental studies is the quality of the data and interpretation scheme, with particular emphasis on the latter. This is because in most modern applications, it is not sufficient to map the conductive targets only, but also to measure their volume, delineate and characterize the hosting structures and cover materials, measure the volumetric water content, the differences in water conductivity due to pollution etc.

Due to the rather involved physics of the TEM method, the existing analysis and interpretation software is relatively limited, both in numbers and availability. In general one can find: (1) High cost

commercial software from a handful of manufacturers. (2) Extreme scarcity of open source software. In fact, the author only knows of the MATLAB forward code by Ingeman-Nielsen and Baumgartner (2006) and the old inversion codes of Walter Anderson; the latter are written in plain FORTRAN and are available from the USGS (Anderson, 1982a-c), but cannot be put to work by a person unfamiliar with old and contemporary editions of FORTRAN, let alone the complete absence of a visual presentation of the results. (3) Limited availability of inversion software, which is usually offered as an executable, without (or with limited) data management and display facilities; this is usually provided by academic institutions, e.g. the University of Oulu, Finland and the University of Aarhus, Denmark.

With the above two exceptions aside, the academic free software community has hitherto not produced remedies. The software presented herein, *maTEM (MAtlab Transient ElectroMagnetics),* marks the beginning of an effort to create an advanced TEM analysis and interpretation package, which may also be expandable and customizable to the needs of a particular user, with little programming effort. Although easy to say, this would be a truly demanding and ambitious undertaking, had it not been for the existence of powerful, general purpose computing engines. On this basis, the realization of such a project is feasible because a computing engine will generally provide a complete high level programming environment, inclusive of graphics, which facilitates the development of advanced software because all the complexities pertaining to low level interfacing, programming and functionality are taken care by the engines themselves. This is much easier and faster than building programs from scratch in some conventional high level language such as C, C++ or FORTRAN.

2. Specifications and programming environment

A modern program, like maTEM aspires to be, should be able to offer a complete solution to the problem of analysis, interpretation and visualization of TEM survey data, allowing the user to:

1. Import and handle *multiple* TEM sounding data, i.e. from more than one sounding locations and more than one type of instruments.
2. Visualize and inspect the data.
3. Process the data with utilities enabling noise suppression, smoothing etc.
4. Perform fast approximate inversions (inverse mappings). These may assist in the interpretation effort, but their primary function would be to provide insight and guidelines for the design of 1-D interpretative models.
5. Design 1-D interpretative models.
6. Perform interactive, 1-D forward modelling and/or inversion for each sounding separately.
7. Perform simultaneous inversion of multiple soundings, either 2-D, or 1-D with application of lateral constraints (in quasi-layered earth structures this amounts to proxy-2D inversion).
8. Display the interpretation in the form of resistivity cross-sections with publication quality graphics; moreover, generate composite displays by overlaying more than one cross-sections.
9. Have the data and results organized in a data base in an automated and transparent manner, so that he/she may be able to concentrate on the analysis only.
10. Be able to repeat any one of the steps 1-9 above at *any* time, in order to improve/ correct the interpretation and seamlessly introduce the results into the data base.

The realization of these specifications requires an appropriate programming and computational environment and careful selection of the interpretation (modelling and inversion) approach.

General purpose scientific computing engines are not many: The most commonly available are the proprietary IDL™ and MATLAB™ and the freeware OCTAVE and SCILAB. Of course, there is an abundance of other (proprietary or non-proprietary) scientific data analysis software, which is generally not suitable, as it is usually specialized (e.g. statistical analysis, curve fitting, data modelling, graphics etc.) and does not provide a sufficiently general and versatile enough programming environment for the development of integrated and advanced software. Of all those, MATLAB™ is the most widespread, diverse and versatile to such an extent, that it has become the *de facto* standard in scientific and technical computing.

MATLAB was not available until the later part of the 1980's, and prior to that, FORTRAN was the language of choice for serious numerical computation. C was making its first steps towards establishing a foothold in the world of scientific computation, but it didn't offer built-in facilities for doing complex arithmetic and this was a serious drawback. Conversely, FORTRAN lacked some of C's advantages such as structures, pointers, and dynamic memory allocation.

The appearance of MATLAB and its imitators made a big impact in the scientific community. MATLAB was originally written to provide easy access to matrix software developed by the LINPACK and EISPACK projects, familiar to FORTRAN programmers for being robust collections of tools for linear algebra. To do this, MATLAB also introduced a new vector-oriented programming language, an interactive environment, and built-in graphics. These features offered many advantages and boosted productivity in comparison to more traditional application development environments. Since, MATLAB has evolved to embed a large collection of state-of-the-art numerical tools, high quality graphics, object-oriented extensions, a built-in interactive debugger, web services and a host of other facilities. Of course, C and FORTRAN have also evolved, with some advanced editions also offering high-level (visual) application development environments. However, neither offers as many treats as MATLAB, graphics for instance being a major issue.

The requirement for a suitable and accurate modelling and inversion method is quite more difficult due to the scarcity of the publicly available software. Anderson's (1982a-c) pioneering FORTRAN codes are robust but insufficient because they deal only with the single/ coincident loop and central loop configurations. Karmis (2003) has developed FORTRAN programs to perform inversion of single- and multiple sounding data, which he has dubbed "*pointem*" and "*linetem*" respectively. While maTEM was being developed, these programs were not publicly available.

The remaining options were either to develop new modeling and inversion code, or, until this is done, to use the program "em1dinv" developed by the Hydro-Geophysics Group of the University of Aarhus, Denmark. This program is well known and tested by the EM geophysical community and is delivered by its author(s) in stand-alone executable form, upon application. It may perform inversion of single or multiple soundings simultaneously; in the latter case, by introducing lateral constraints between soundings, i.e. restraining the variation between homologous layers with respect to each other, it may also perform quasi-2D inversion in layered earth structures (Auken and Christiansen, 2004; Christiansen and Auken, 2004; Auken et al, 2005). An additional important advantage is the possibility to adjust the transmitter waveform to the specifications of different instrument manufacturers. On the downside, the program cannot, at present, handle earth models with complex and frequency-dependent resistivity. Thus, in some cases it may fail to interpret data affected by induced polarization effects. Moreover, because it assumes paramagnetic earth materials, it cannot handle super-paramagnetic phenomena appearing in magnetized or iron-rich soils.

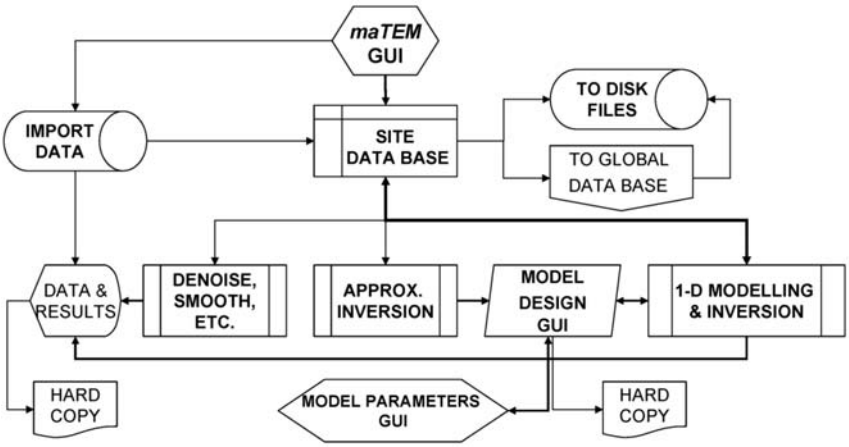

Fig. 1: Flowchart of a data analysis child process.

3. Program architecture

It should be apparent, even to the novice, that the specifications set at the beginning of Section 2, may only be realized by enabling the execution of multiple parallel processes. maTEM is designed so that each one of these processes will comprise the analysis of an individual TEM sounding at a given site (a *data analysis process*). The data and the results are assembled in a site-specific data base (DB). The individual site-DBs, in turn, contribute to the formation of a global-DB which can be independently handled, exported and re-imported. The global-DB also feeds with data and initial earth models the process of for multiple simultaneous inversions and assimilates the results for permanent storage and display. A GUI driven *parent* process, the *maTEM GUI*, controls the *data analysis child processes*. This design philosophy is illustrated and explained in the flowcharts of Figures 1-3.

Fig. 1 shows the (more or less self-explanatory) flow of work and information in a data analysis child process. Data processing (de-noising, smoothing etc.) are controlled by the maTEM GUI; the results are fed back to the site-DB and are hence available for the approximate and 1-D layered modelling and inversion operations. The site-specific Earth Model is designed and handled interactively (graphically) in an independent *Model Design* GUI which, in fact, is *child* of the maTEM GUI. This is supplied with the results of approximate inversion, which can be displayed at the user's discretion. The model design GUI generates a child process, the *Model Parameters GUI*, in which the user may manually introduce layer resistivities, thicknesses and most importantly, vertical and lateral constraints for the inversion. The site-DB can be exported in the form of a sounding data file (tem-file) and a sounding model file (mod-file).

Fig. 2 shows that the site-DBs of the parallel analysis child processes are collated to form the global-DB, in a manner that will be explained later. At present, the global-DB can be stored as a MATLAB binary file (mat-file). The information necessary for multiple simultaneous inversions (data and initial earth models) is extracted from the global-DB and the results are re-introduced for permanent storage. In addition, the results of the inversions can be extracted from the global-DB and stored independently as an ASCII file, the inv-file, to be available for visual inspection/ editing and display in the form of cross sections. An existing inv-file is not destroyed by subsequent write operations – any new results are merely appended to it, therefore caution should be exercised in order to keep the file free of unwanted repetitions.

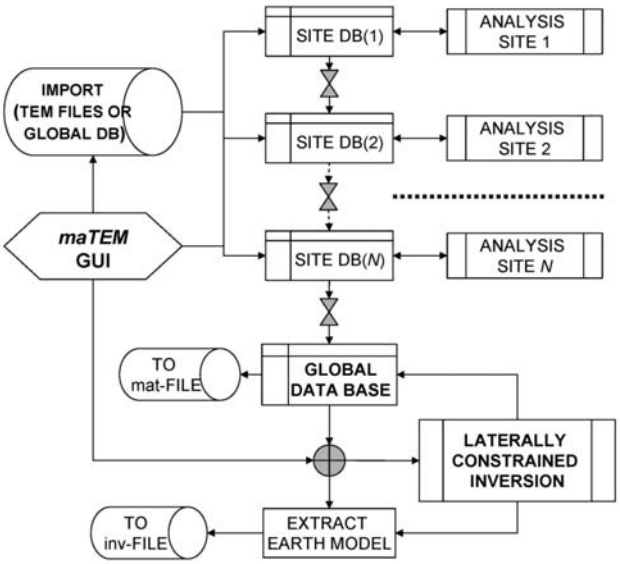

Fig. 2: Outline of the simultaneous analysis of multiple TEM soundings. Each "ANALYSIS" box corresponds to a data analysis child process.

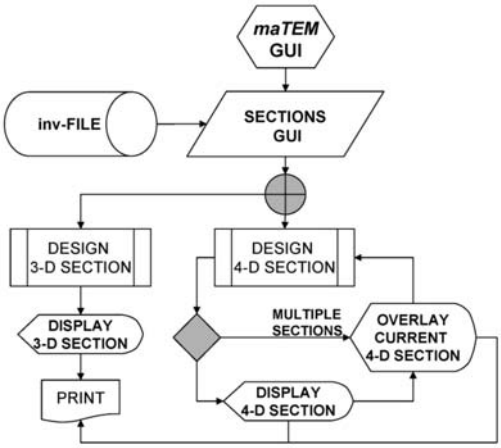

Fig. 3: Flowchart for the construction and display of interpretative cross-sections.

Fig. 3 shows how maTEM constructs and displays interpretative cross sections. The maTEM GUI launches yet another child process, the *Sections GUI*, through which the interpretation is imported from the inv-file, or extracted from the global-DB. The soundings available in the inv-file are displayed in map form and the user congigures the cross-section by pointing and clicking. Cross-sections can be displayed in either 3-D (planar) or 4-D (volume) mode. In the latter case, multiple cross-sections can be overlaid in a single graph, thus enabling visualization of lateral correlations and changes in the geoelectric structure of the entire study area.

As is already clear, maTEM has been designed to be GUI-driven at all levels. This requires object-oriented programming and defines the frame and course of realizing the design specifications. In addition, one has to consider that all child processes must be executed in parallel and that the site- and global-DBs must be updated automatically every time there's some action by the user. Given that in the GUI-driven, object-oriented environment of MATLAB, the information pertaining to modifica-

tions of graphical objects (in our case the graphical representations of data and earth models) is directly accessible through their respective handle structures, the following method for passing information between processes and data bases was adopted:

Let the data comprise $n = 1,\ldots, N$ soundings, with each sounding comprising $m_n = 1,\ldots, M_n$ channels (gates). Then, the handles of the graphical objects can be organized in data constructs comprising *homologous* $1 \acute{} N$ *data structure arrays of data structures*, in such a manner, that the n-th element of a data structure array will comprise a $1 \times M_n$ data structure array whose fields are the handles of the M_n *homologous* graphical objects of the n-th sounding. Given that the m_n*-th* handle is actually a data structure conveying the properties of the graphical object, a strict hierarchy of data structures is thus created, organizing the available information in a manner directly accessible by reference. Any modification of the m_n–th graphical object is registered in the respective m_n–th handle and the hierarchical data construct is instantaneously updated with the new information.

The homologous structure arrays of graphical objects used in maTEM are associated with:

a. Data manipulation and management: This construct contains the graphical objects representing the data of the n-th sounding. It allows the user to hide/show entire soundings for convenience, and, more importantly, to earmark any m_n–th data channel for *de-activation/ re-activation*. The term *de-activation* implies the *exclusion* of the m_n–th data channel from further consideration and is applied to measurements heavily distorted by early time effects or by noise, to the point of being irrecoverable.

b. Error bar manipulation and management: This construct contains the graphical objects representing the *observational error* associated with the m_n–th data channel in the n-th sounding.. It allows the user to hide/show the error bars associated with the data of each sounding separately, thus facilitating the visual inspection and evaluation of individual soundings.

c. Earth Model manipulation and management: This construct contains the handles of the graphical objects representing the 1-D geoelectric structural model used for the interpretation of the n-th sounding and is displayed in the "Model Design GUI".

d. Inversion parameters management: This contains the vertical and horizontal constraints applied to the inversion of the n-th model during the interpretation of the n-th sounding.

The site-DB is a data structure whose fields are alphanumeric and numeric constants and arrays containing all the useful information pertaining to an individual sounding. This includes survey-and-site-related information from the header(s) of the sounding data file, site coordinates, Tx/Rx size(s) and configuration, ramp duration, the channel central times, the sounding data in the form of impulse response, late-time apparent resistivity and true resistivity with associated uncertainties, the earmarks of the deactivated data channels, the approximate inverses, the interpretative 1-D Earth model and the associated theoretical response curves. It should be expected that the global-DB would be a $1 \times N$ data structure array of the site-DB data structures, symbolically named $\mathbf{D}(n)$. When some graphical object pertaining to the n-th sounding data or model parameters is interactively modified during the course of the analysis, the corresponding field of the $\mathbf{D}(n)$ is automatically updated via the pertinent handle. Likewise, if, after such a modification an approximate inversion or layered 1-D modeling or inversion is executed, the pertinent fields of $\mathbf{D}(n)$ are automatically updated by direct substitution of the results. The global-DB can be exported as a MATLAB mat-file, together with the ":inversion parameters" construct. This amounts to saving the analysis session. Re-importing the global-DB amounts to re-instating the session at the point at where it has been saved. This is an effective way to ensure the seamless continuity of work.

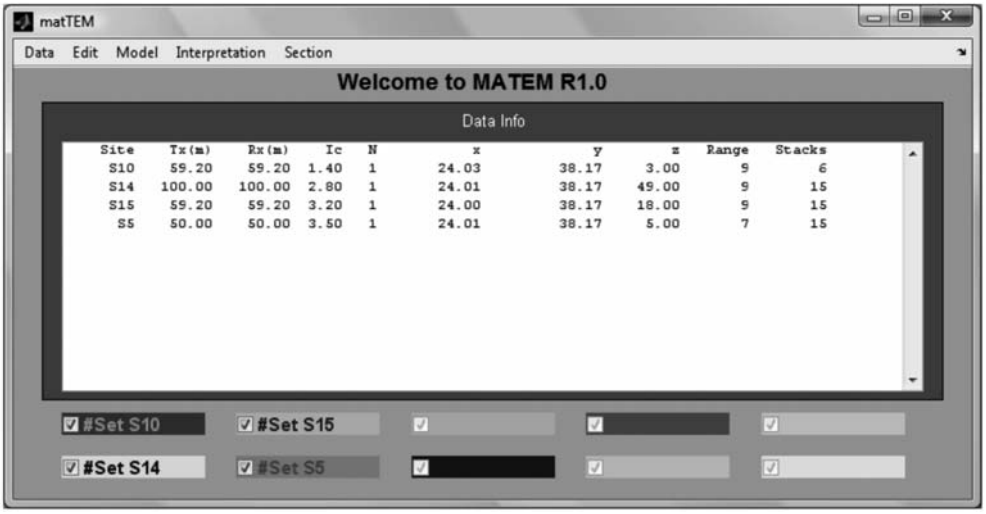

Fig. 4: The maTEM GUI after importation of data from four soundings collected with the TEM-FAST 48 system. The GUI displays key information about the soundings.

Every other graphical object not included in the above description is assigned with a unique *identification tag"*, using the 'tag' property of the object. The retrieval and registering of information in these objects is based upon acknowledgement of their ID tag. Finally, it should be noted that maTEM also features a collection of constants (keywords) and variables by which the user can choose between different modes of data and model displays, and tune the execution of em1dinv. The assignment of these parameters is also GUI driven and they can change during the course of analysis (runtime variables). They are organized in yet another global data structure whence they are passed to the appropriate calling routine. The specification and explanation of these variables is beyond the scope of this work.

4. Implementation

The maTEM GUI can be seen in Fig. 4, after a data set has been imported for analysis. The "Data" menu facilitates importation/ exportation of data and results, as well as general functions pertaining to the mode of data display (impulse response or apparent resistivity) and the type of the coordinates adopted for the survey. At present maTEM may accept the following types of data:

— Multiple *single-site* TEM data files in the TEM-FAST 48, AMIRA and em1dinv formats (each file contains one sounding).

— Multi-site TEM data files in the TEM-FAST 48 and AMIRA formats (each file contains more than one soundings)

— maTEM mat-files (i.e. the global-DB) in MATLAB binary format.

Upon importation the maTEM GUI displays important information as per Fig. 4. The (coloured) boxes indicate the colour associated with the data and models of each sounding and the checkboxes can be used to hide/ show the respective soundings for convenience.

The data is displayed in the "DATA" window as per Fig. 5a; this also comprises a GUI with menus

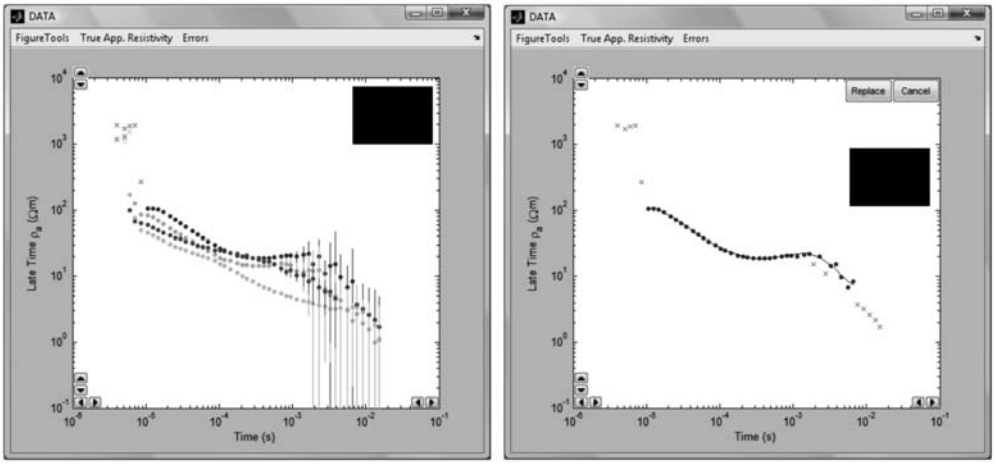

Fig. 5: (a) The four soundings shown in Fig.4, displayed as late time apparent resistivities. (b) Sounding with concealed errors, deactivated channels (x-markers) and a smooth model (continuous line) computed with a 9th order exponential spectrum and pending acceptance.

facilitating concealment/ projection of true apparent resistivity curves and error bars. The "Edit" menu offers de-noising and smoothing utilities. At this point de-noising comprises the de-activation of distorted data channels. This is done by pointing and clicking on the graphical representation of a data channel (solid circle). A deactivated channel is marked with x and may be re-activated in the very same way. Smoothing is possible with least squares smoothing splines (e.g. Wahba, 1990) or by fitting the decaying impulse response data with a function of the form

and recalculating the late time and true apparent resistivities (exponential spectrum method). An example is shown in Fig. 5b.

The "Model" menu initializes the Model Design GUI, in which layered Earth models can be created and manipulated via the dedicated "Handle" menu (Fig. 6). The models are introduced graphically, by pointing and clicking; for convenience and precision, the cursor coordinates (depth and resistivity) are indicated at the bottom of the Model Design GUI. The results of approximate inversion may also be overlaid to assist in the design. A model can be updated with insertion or deletion of layers and can be modified by capturing and shifting the breakpoints of the model (solid squares in Fig. 6 and 7a) with the mouse. There can be one layered model per sounding.

Upon completion of the graphical construction of an Earth model, the respective "Model Parameters GUI" is displayed. This, offers additional means of controlling the interpretation by allowing the manual fine-tuning of the model resistivities and thicknesses, as well as the definition of "prior information weights" (to fix or restrain the variation of a parameter depending on the existence of independent information), vertical constraints (restrain the variation between consecutive layers), and horizontal constraints (restrain the variation of homologous layers in neighbouring soundings during laterally-constrained inversion of multiple soundings along profiles).

The menu "Interpretation" is used to compute approximate inverses with the methods of Barsukov

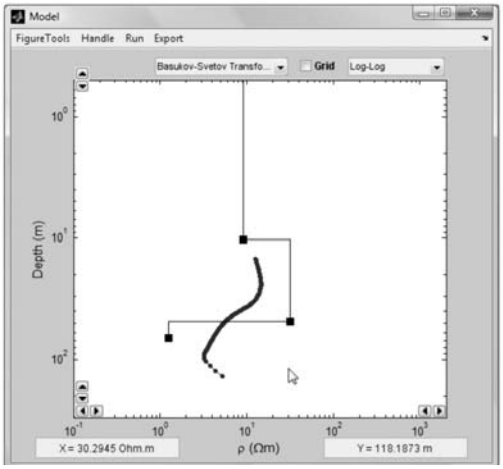

Fig. 6: The Model Design GUI during the graphical construction of a layered earth model

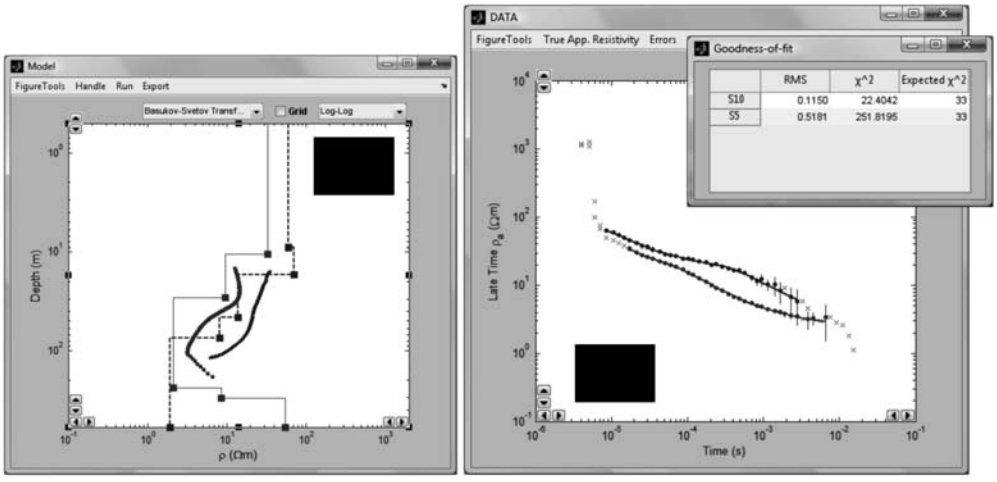

Fig. 7: Simultaneous inversion of two soundings. (a) The final models are displayed in the Model Design GUI; approximate inverses are overlaid for comparison. (b) The model theoretical responses (continuous lines) are laid over the measured data. The "Goodness-of-fit" window displays the corresponding RMS and χ^2 metrics.

and Svetov (Barsukov et al, 2007) or S-inversion (Tartaras et al, 2000), to perform interactive forward modelling and inversion and to adjust the source waveform and the control parameters necessary for the execution of em1dinv. The latter (modelling and inversion) is also possible – and more versatile – via the "Run" menu of the Model Design GUI (Fig. 6 and 7a). Interactive forward modelling can be done either by capturing and shifting the breakpoints of the model (solid squares in Fig. 6 and 7a) with the mouse, or by typing the updated model parameters in the appropriate boxes of the Model Parameters GUI. The progress of the modelling exercise and the quality of the interpretation is monitored both visually and numerically by means of the RMS and c^2 metrics projected on a separate, "Goodness-of-fit" window (Fig. 7b). Only one sounding can be modelled at a time in this manner. Conversely, more than one sounding can be inverted simultaneously, with or without vertical and lateral constraints. Fig. 7 displays the result of such an exercise for two de-noised soundings (S5 and S10 in Fig. 4). The results of the interpretation may be exported in the various available

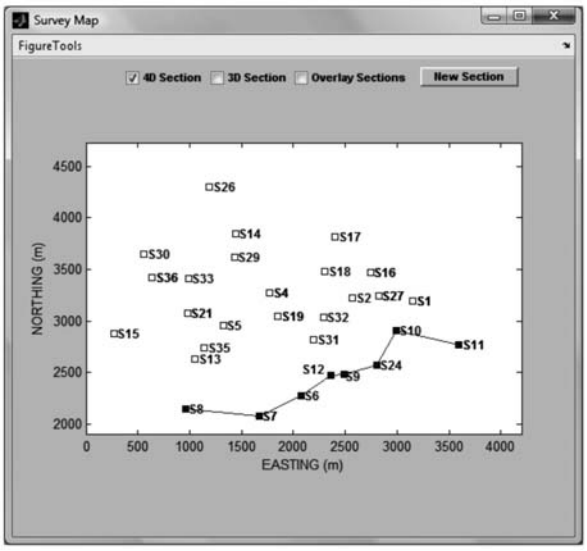

Fig: 8. The "Survey Map" GUI, used for designing a cross section.

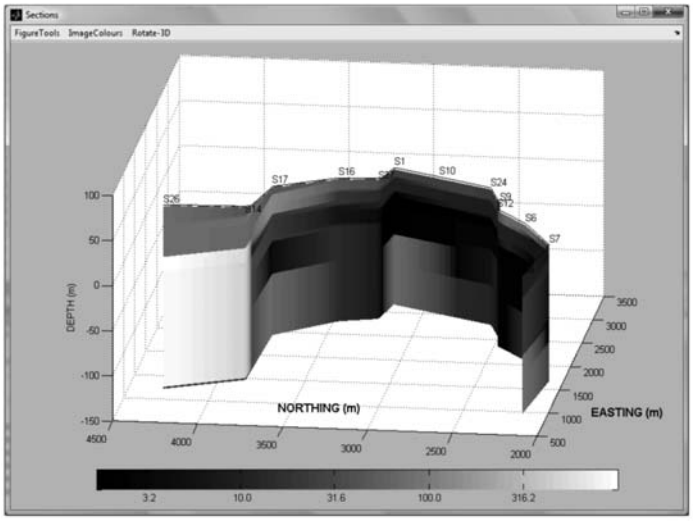

Fig. 9: A 4-D (volume) representation of two sections joined at S1, as viewed from the NE.

formats, via the "Export" menu of the Model Design GUI, or the appropriate menu entry under the "Data" menu of the maTEM GUI.

Finally, the menu "Section" allows the user to import the results of the interpretation from an inv-file and to build interpretative cross-sections. The locations of the interpreted soundings are displayed in the "Survey Map" GUI (open squares in Fig. 8), where the user may design the section by selecting the mode of presentation (3D or 4D) and pointing and clicking on the desired sounding locations. When in three-dimensional (4D) display mode, sections can be overlaid (multiple sections can be displayed on the same graph) as per Fig 9; they can also be freely rotated (menu "Rotate-3D") in Fig. 9, and redrawn with a variety of different colour schemes (menu "ImageColors" in Fig. 9).

5. Epilogue

At the present stage of development maTEM provides a relatively broad and functional range of tools for the analysis of any type of TEM data (single loop, coincident loop and offset configurations). Overall, it offers a decent and in several aspects advanced and versatile means of treating TEM data, and may even stand competitively against commercial analysis programs.

Nevertheless, one can think many additional tools that can be included in future releases. One can think of several improvements in the code, addition of more advanced processing techniques and graphical utilities etc. One important development may be the incorporation of a means to model data with induced polarizaton effects. This would certainly increase the range of applications for the benefit of the user.

Another very important point, as well as one for which very few remedies exist, is the joint (mutually constrained) interpretation of different geophysical prospecting methods. It is common knowledge that every individual electrical or electromagnetic prospecting method is subject to physical limitations that restrain its scope of application. It is also common knowledge that two or more methods jointly applied and interpreted, are much more effective because they may compensate for each other's limitations. However, the geophysical software community is reacting slowly to the dearth of software solutions, at least in the public domain.

Em1dinv is one shiny exception: it is a pioneering application and very handy in this respect, because in addition to any kind of TEM loop configuration, it may handle dc resistivity data (Schlumberger and Wenner arrays), controlled-source frequency domain EM (FEM) and natural field EM (AMT/MT) sounding data in any combination. maTEM has an architecture readily expandable to incorporate any number of additional data analysis processes (different prospection methods) and thus can be expanded to meet the challenge of mutually constrained geophysical data analysis with relatively minor programming effort.

Finally, maTEM may be available from the author upon request, subject to the applicant having secured a license to use em1dinv from its own authors. For an application to use em1dinv see http://www.geofysiksamarbejdet.au.dk/page559.aspx.

6. Acknowledgments

The author acknowledges limited support by the "Kapodistrias Programme" of the *Research Grants Secretariat,* National and Kapodistrian University of Athens. Ms Eleftheria Drosopoulou has *significantly* assisted in the development of this program, as part of her Postgraduate Dissertation at the Department of Geophysics and Geothermy, NKUA.

7. References

Anderson, W.L., 1982a. Calculation of transient soundings for a coincident loop system (Program TCOLOOP). *USGS* Open-File Report 82-378.

Anderson, W.L., 1982b. Nonlinear least-squares inversion of transient soundings for a coincident loop system (Program NLSTCO), *USGS* Open-File Report 82-1064

Anderson, W.L., 1982c. Nonlinear least-squares inversion of transient soundings for a central induction loop system (Program NLSTCI), *USGS* Open-File Report 82-1129

Auken E. and Christiansen A.V. 2004. Layered and laterally constrained 2D inversion of resistivity data. *Geophysics* 69, 752–761.

Auken, E., Christiansen, A.V., Jacobsen, B.H., Foged, N. and Sørensen, K.I., 2005. Piecewise 1D laterally constrained inversion of resistivity data, *Geophysical Prospecting*, 53, 497–506.

Barsukov, P.O., Fainberg, E.B. and Khabensky, E.O., 2007. Shallow investigations by TEM-FAST technique: Methodology and examples, in V.V. Spichak (editor), *Methods in Geochemistry and Geophysics, Volume 40,* 56-77.

Christiansen, A. V. and Auken, E., 2004: Optimizing a layered and laterally constrained 2D inversion of resistivity data using Broyden's update and 1D derivatives. *Journal of Applied Geophysics*, 56, 247-261.

Ingeman-Nielsen, T. and Baumgartner, F. 2006. CR1Dmod: A Matlab program to model 1D complex resistivity effects in electrical and electromagnetic surveys. *Computers & Geosciences,* 32, 1411–1419

Karmis, P., 2003. Automated interpretation of transient electromagnetic soundings. Doctoral Dissertation, N.K University of Athens (in Greek).

Tartaras, E., Zhdanov, M.S. Wada, K. Saito, A. and Hara, T., 2000. Fast Imaging of TDEM data based on S-inversion. *Journal of Applied Geophysics,* 43, 15–32.

Wahba, G., 1990. Spline models for observational data. In: *CBMS-NSF Regional Conference Series in Applied Mathematics* 59, Soc. Industrial and Applied Mathematics, Philadelphia, Pennsylvania (1990), p. 169.